Seeing Is Not Always Believing: ISAC-Assisted Predictive Beam Tracking in Multipath Channels

Yanpeng Cui, *Student Member, IEEE*, Qixun Zhang, *Member, IEEE*, Zhiyong Feng, *Senior Member, IEEE*, Qin Wen, Zhiqing Wei, *Member, IEEE*, Fan Liu, *Member, IEEE*, and Ping Zhang, *Fellow, IEEE*

***Abstract*—The integration of sensing and communications (ISAC) has brought considerable benefit in predictive beamforming. However, it is dedicated to the line-of-sight channels, and the effect of the spatial degree of freedom (DoF) of multipath channels on it has not been revealed. This letter proposed a novel ISAC-assisted beam-tracking solution in multipath channels. Based on the reflected echoes, the kinematic parameters are measured and the extended Kalman filtering (EKF) is designed for angle prediction. The fine beam tracking method is also proposed based on the tracking results of the EKF. Simulation results show that the proposed method has a remarkable superiority over the conventional feedback-based one. In addition, the angle parameters observed from radar echoes are not always the optimal alignment direction, which still has gaps from the global optimal performance in the multipath channel, and this gap can be bridged by the proposed fine beam tracking method.**

***Index Terms*—Integration of sensing and communications (ISAC), Multipath channel, Beam tracking, Extended Kalman filtering, UAV communication.**

I. Introduction

With the deep integration of wireless communications and aerial vehicular technology, we are at the dawn of the era of ubiquitous aerial networks [1]. The Millimeter-wave (mmWave) communication with its abundant spectrum resource has the potential to support the high-throughput and low-latency requirements of various UAV application scenarios. To compensate for the high path loss in mmWave-UAV communications, it is significant to generate narrow beams at the ground base station (BS) and align toward UAVs to achieve high array gains. However, it's not an easy task due to the highly dynamic mobility of UAVs.

Conventional beam alignment solutions rely on communication feedback called beam training. By transmitting a few pilots embedded in the downlink signal towards a few directions, the channel states can be estimated and then the optimal aligned angle can be interactively found [2]. It generally suffers from tedious feedback and the consequent delay, and the fleeting opportunities for alignment may thus slip away. In view of this, several pioneering contributions have discussed the integration of sensing and communications (ISAC)-based predictive beamforming methods [3], which brings large gains in beam tracking. Besides, it has been demonstrated that it is capable of reducing the overheads by up to 43.24% based on the fifth-generation (5G) New Radio (NR) frame structure [4], since the tedious dedicated downlink pilots and uplink feedback are removed via processing the reflected echoes.

While these ISAC-based solutions were well-designed with tailor-made algorithms, they generally assume a simplistic Line-of-Sight (LoS) channel, and things will become more complex in practical multipath scenarios. An explicit LoS path is required to ensure sensing performance in most cases, and echoes reflected by the unintended target (i.e., clutter) may induce sensing errors of the intended one. By contrast, both the LoS and non-LoS (NLoS) paths are communication-friendly since a higher spatial degree of freedom (DoF) can be attained by utilizing them [5]. Accordingly, the alignment direction with the highest signal-to-noise ratio (SNR) may deviate from both the actual angles between transmitter and receiver, and the angles sensed from echoes with inherent errors. Following the spirit of "seeing is not always believing", the above fundamental effect brought by multipath channels may lead to a gap between the optimal rate and the one achieved by ISAC. By noting this, it is of pivotal importance to illuminate three questions in the multipath channel: i) how much benefit will the ISAC-based beam tracking solution enjoy compared to the feedback-based one? ii) how much further is the ISAC-based performance from the maximum rates? iii) how many efforts should be made to achieve the maximum rates?

This compact letter takes a meaningful step forward toward ISAC-assisted beamforming in more realistic environments. Our aim is to design a novel ISAC-assisted beam-tracking solution in multipath channels. Explicitly, an ISAC-enabled BS is considered to perform beamforming toward an aerial communication user, whose kinematic parameters are also sensed by the reflected echoes. To provide accurate beam tracking during long-term moving, an extended Kalman filtering (EKF) is designed for angle prediction. For the EKF-ISAC, we shed light on its superiority to the feedback-based one and found that the angle parameters observed from radar echoes are not always the optimal alignment direction, which still has nearly a one-third gap from the global optimal performance in multipath channel. To bridge this gap, the fine beam tracking

Manuscript received 28 June 2023; revised 7 August 2023; accepted 8 August 2023. Date of publication 10 August 2023; date of current version 9 January 2024. This work was supported in part by the Major Research Projects of NSFC under Grant 92267202; in part by the National Key Research and Development Project under Grant 2020YFA0711303; and in part by the BUPT Excellent Ph.D. Students Foundation under Grant CX2022208. The associate editor coordinating the review of this article and approving it for publication was D. Mishra. *(Corresponding author: Zhiyong Feng.)*

Yanpeng Cui, Qixun Zhang, Zhiyong Feng, Zhiqing Wei, and Ping Zhang are with the School of Information and Communication Engineering, Beijing University of Posts and Telecommunications, Beijing 100876, China (e-mail: cuiyanpeng94@bupt.edu.cn; zhangqixun@bupt.edu.cn; fengzy@bupt.edu.cn; weizhiqing@bupt.edu.cn; pzhang@bupt.edu.cn).

Qin Wen is with the School of Computer Science, Northwestern Polytechnic University, Xi'an 710072, China (e-mail: wqnwpu@mail.nwpu.edu.cn).

Fan Liu is with the Department of Electronic and Electrical Engineering, Southern University of Science and Technology, Shenzhen 518055, China (e-mail: liuf6@sustech.edu.cn).

Digital Object Identifier 10.1109/LWC.2023.3303949

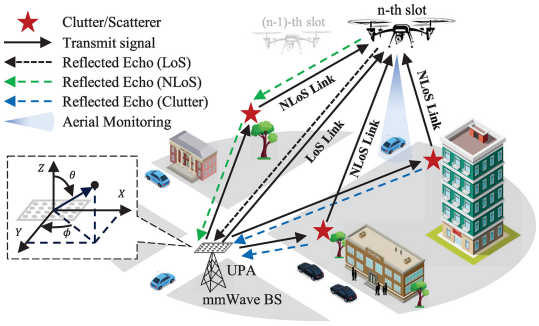

Fig. 1. The typical scenario of the mmWave UAV network with multipath.

method is proposed based on the prediction result of EKF-ISAC, and one can obtain the intended performance from the tradeoff between achievable rate and time efficiency.

II. System Model

As shown in Fig. 1, we consider a cellular-connected UAV network that operates at mmWave frequency. The ground BS is equipped with a mmWave massive MIMO (mMIMO) uniform planar array (UPA) consisting of N_t transmit antennas and N_{r_b} receive antennas, ensuring that the signal echoes for sensing can be received while maintaining uninterrupted downlink communications concurrently. The consequent difference in the receiving and transmitting angles can be compensated by the relative position of these two UPAs. The small angle difference between the received and transmitted beams caused by the separated antennas can be compensated by their relative positions. The 3-D location vectors of the BS and the UAV at the n-th slot are denoted as $\mathbf{p}_b = [\mathrm{p}_b(1), \mathrm{p}_b(2), \mathrm{p}_b(3)]^T$ and $\mathbf{p}_n = [\mathrm{p}_n(1), \mathrm{p}_n(2), \mathrm{p}_n(3)]^T$. The Euclidean distance between them is denoted as $d_{n,0} = ||\mathbf{p}_n - \mathbf{p}_b||$. Moreover, the UPA is also assumed to be deployed at the bottom of UAVs. In what follows, we will describe the communication and sensing models and their channel impulse response (CIR).[1]

Remark 1: Note that our proposed techniques can be applied to multi-user scenarios by beam association, which can be easily realized by the task assignment algorithm, e.g., Kuhn-Munkras algorithm and vampire bat optimizer [2]. Given the page limit, we designate the discussion of the multi-UAV network as our future work.

A. Communication Model

Here we employ the channel model for communication in the urban microcell scenario [6], and the LoS probability is

$$\mathrm{P_{LoS}} = \begin{cases} 1, & \text{if } d_{n,0}^{\mathrm{2D}} \le 18\,\mathrm{m} \\ 18/d_{n,0}^{\mathrm{2D}} + (1 - 18/d_{n,0}^{\mathrm{2D}})e^{-d_{n,0}^{\mathrm{2D}}/p_1}, & \text{otherwise} \end{cases} \quad (1)$$

where $d_{n,0}^{\mathrm{2D}}$ denotes the horizontal component of $d_{n,0}$, and $p_1 = 233.98 \times \log_{10}(\mathrm{p_n}(3)) - 0.95$. If the LoS path exists, the communication CIR can be modeled as $\mathbf{H}_n = \sqrt{\mathrm{K_R}}\mathbf{H}_n^{\mathrm{L}}/\sqrt{\mathrm{K_R}+1} + \mathbf{H}_n^{\mathrm{N}}/\sqrt{\mathrm{K_R}+1}$, where $\mathbf{H}_n^{\mathrm{L}} = \beta_{n,0}e^{j2\pi\gamma_{n,0}t}\delta(t-\tau_{n,0})\mathbf{u}_{n,0}\mathbf{a}_{n,0}^H$ and $\mathbf{H}_n^{\mathrm{N}} = \sum_{k=1}^{K}\sum_{l=1}^{L}\beta_{n,k,l}e^{j2\pi\gamma_{n,k,l}t}\delta(t-\tau_{n,k,l})\mathbf{u}_{n,k,l}\mathbf{a}_{n,k,l}^H$ are the LoS and NLoS components of $\mathbf{H}_n$, respectively. Symbols $\mathrm{K_R}$, K and L denote the Ricean K-factor, the number of clusters, and the number of paths in each cluster, respectively. We remark here that $\mathrm{q}_{n,0}$ and $\mathrm{q}_{n,k,l}$ respectively represent the parameter "q" of the LoS path and the l-th NLoS path in the k-th cluster. Symbols γ and τ are the Doppler shift and delay of paths, and $\beta_{n,0}$ and $\beta_{n,k,l}$ are the zero-mean Gaussian fading coefficients with variance $\sigma_{\beta_{n,0}}$ and $\sigma_{\beta_{n,k,l}}$, and we have $10\log_{10}(\sigma_{\beta_{n,0}}) = -\mathrm{PL}_{n,0} - \mathrm{SF}_{n,0}$ and $10\log_{10}(\sigma_{\beta_{n,k,l}}) = -\mathrm{PL}_{n,k,l} - \mathrm{SF}_{n,k,l}$, where PL denotes the path loss.[2] The shadow fading $\mathrm{SF}_{n,0}$ and $\mathrm{SF}_{n,k,l}$ are Gaussian distributed with zero mean and variance $\sigma_{\mathrm{SF}_{n,0}}$ and $\sigma_{\mathrm{SF}_{n,k,l}}$, respectively.

The array steering vector of the BS's transmit UPA, namely $\mathbf{a}(\phi,\theta) \in \mathbb{C}^{N_t \times 1}$, is defined as $[\mathbf{a}]_{(n_{\mathrm{t_y}}-1)N_{\mathrm{t_x}}+n_{\mathrm{t_x}}} = e^{j\pi\sin\theta[(n_{\mathrm{t_x}}-1)\cos\phi+(n_{\mathrm{t_y}}-1)\sin\phi]}/\sqrt{N_t}$, where we assume the UPA has half-wavelength spacing among $N_t = N_{\mathrm{t_x}} \times N_{\mathrm{t_y}}$ antennas. Symbols $n_{\mathrm{t_x}} = 1,\ldots,N_{\mathrm{t_x}}$, $n_{\mathrm{t_y}} = 1,\ldots,N_{\mathrm{t_y}}$ denote the number of antenna along axis x and y. Symbols ϕ,θ in $\mathbf{a}(\phi,\theta)$ denote the azimuth direction-of-departure (ADoD) and the elevation DoD (EDoD). Symbols $\mathbf{a}_{n,0}$ and $\mathbf{a}_{n,k,l}$ denote the transmit steering vector for the LoS and NLoS paths, respectively. The steering vector of the UAV's receive UPA, namely $\mathbf{u}(\phi',\theta')$, is similarly defined as $\mathbf{a}(\phi,\theta)$ with N_{r_u} receive antennas on the UAV, where ϕ',θ' denote the azimuth direction-of-arrival (ADoA) and the elevation DoA (EDoA). For the NLoS path, the ADoA can be calculated by $\phi'_{n,k,l} = \phi'_{n,k} + c_{ASA}\alpha_{n,k,l}$, where $\phi'_{n,k}$ is the mean of the ADoA in the k-th cluster, c_{ASA} is the cluster-wise root-mean-square DoA spread, and $\alpha_{n,k,l}$ is the ray offset DoA [7]. The EDoA $\theta'_{n,k,l}$, the ADoD $\phi_{n,k,l}$, and the EDoD $\theta_{n,k,l}$ are generated in a similar way as $\phi'_{n,k,l}$.

By denoting the transmitted data at the n-th slot and time t as $s_n(t)$, the beamformed signal can be given as $\mathbf{s}_n(t) = \mathbf{f}_n s_n(t)$, where $\mathbf{f}_n$ denotes the transmit beamforming vector and $s_n(t) = \sum_{p=0}^{P-1}\sum_{q=0}^{Q-1} s_{p,q}e^{j2\pi i\Delta f(t-qT_s)}$ is the OFDM signal. Symbols P, Q and Δf denote the number of sub-carriers, number of symbols and sub-carrier spacing in $s_n(t)$ and $s_{p,q}$ denote the transmitted data on the p-th sub-carrier of the q-th symbol. The total duration of an OFDM symbol is defined as $T_s = T_{cp} + T$, where T_{cp} and T denote the cyclic prefix duration and the elementary symbol duration, respectively. The signal received by UAV via a receive beamformer $\mathbf{w}_n$ is given by $\mathbf{r}_n(t) = \kappa\sqrt{p_n}\mathbf{w}_n^H\mathbf{H}_n\mathbf{f}_n s_n(t) + \mathbf{z}_c(t)$, where $\kappa = \sqrt{N_t N_{r_u}}$, and p_n represents the transmit power, and $\mathbf{z}_c(t)$ is the zero-mean Gaussian noise with variance σ_c^2. Assuming that the ISAC signal has a unit power, the transmit SNR and the receive SNR are expressed as $\Gamma_t = p_n/\sigma_c^2$

[1] Fig. 1 is only a schematic diagram to show that various types of scatterers have different impacts on communication and sensing. In the following design and simulations, the types and locations of scatterers are randomly defined and generated, no matter which side they belong to.

[2] According to [7], for the LoS path, we have $\mathrm{PL}_{n,0} = 32.4 + 21\log_{10}(d_{n,0}) + 20\log_{10}(f_c)$, if $10\,\mathrm{m} \le d_{n,0}^{\mathrm{2D}} \le D_n$, otherwise $\mathrm{PL}_{n,0} = 32.4 + 40\log_{10}(d_{n,0}) + 20\log_{10}(f_c) - 9.5\log_{10}(D_n^2 + (\mathrm{p}_n(3) - \mathrm{p}_b(3))^2)$, if $D_n < d_{n,0}^{\mathrm{2D}} \le 5\,\mathrm{km}$. Symbol $D_n = 4(\mathrm{p}_b(3) - 1)(\mathrm{p}_n(3) - 1)f_c/c$ denotes the break-point distance, where f_c and c are the carrier frequency and the speed of light, respectively. For the NLoS paths, we have $\mathrm{PL}_{n,k,l} = 32.4 + 31.9\log_{10}(d_{n,0}) + 20\log_{10}(f_c)$.

and $\Gamma_r = p_n|\kappa \mathbf{w}_n^H \mathbf{H}_n \mathbf{f}_n|^2/\sigma_c^2$. The achievable rate can be formulated as $R_n = \log_2(1+\Gamma_r)$.

B. Sensing Model

For the mono-static sensing system deployed in BS, we assume that the LoS path, namely the direct target returns, and the NLoS paths, can both provide the required sensing information [8], which is different from the communication CIR. Therefore, the sensing CIR can be denoted as $\tilde{\mathbf{H}}_n = \tilde{\mathbf{H}}_n^{\mathrm{L}} + \tilde{\mathbf{H}}_n^{\mathrm{N}} + \tilde{\mathbf{H}}_n^{\mathrm{C}}$, where $\tilde{\mathbf{H}}_n^{\mathrm{L}} = \tilde{\beta}_{n,0} e^{j2\pi\tilde{\gamma}_{n,0}t}\delta(t-\tilde{\tau}_{n,0})\mathbf{b}_{n,0}\mathbf{a}_{n,0}^H$, $\tilde{\mathbf{H}}_n^{\mathrm{N}} = \sum_{\tilde{k}=1}^{\tilde{K}}\sum_{\tilde{l}=1}^{\tilde{L}} \tilde{\beta}_{n,\tilde{k},\tilde{l}} e^{j2\pi\tilde{\gamma}_{n,\tilde{k},\tilde{l}}t}\delta(t-\tilde{\tau}_{n,\tilde{k},\tilde{l}})\mathbf{b}_{n,\tilde{k},\tilde{l}}\mathbf{a}_{n,\tilde{k},\tilde{l}}^H$ and $\tilde{\mathbf{H}}_n^{\mathrm{C}} = \sum_{\tilde{\theta}_i,\tilde{\phi}_i\in\mathbf{\Omega}} \tilde{\beta}'_{n,i} e^{j2\pi\tilde{\gamma}'_{n,i}t}\delta(t-\tilde{\tau}'_{n,i})\mathbf{b}_{n,i}\mathbf{a}'^H_{n,i}$ denote the LoS, NLoS and clutter components, respectively. Symbols $\tilde{\beta}_{n,0} = \epsilon_{n,0}(2d_{n,0})^{-2}$, $\tilde{\gamma}_{n,0}$ and $\tilde{\tau}_{n,0}$ denote the reflection coefficient, Doppler frequency, and delay of the target UAV of the LoS sensing path, respectively. Symbol $\epsilon_{n,0}$ is the complex radar cross-section. Besides, symbols $\tilde{\beta}_{n,\tilde{k},\tilde{l}}$, $\tilde{\beta}'_{n,i}$, $\tilde{\gamma}_{n,\tilde{k},\tilde{l}}$, $\tilde{\gamma}'_{n,i}$, $\tilde{\tau}_{n,\tilde{k},\tilde{l}}$ and $\tilde{\tau}'_{n,i}$ have the similar meaning as the above parameters, the only difference is that the symbols $\tilde{\mathrm{q}}_{n,\tilde{k},\tilde{l}}$ and $\tilde{\mathrm{q}}'_{n,i}$ are respectively the parameters of the $\tilde{l}$-th scatterer of the $\tilde{k}$-th cluster and the i-th clutter, where "$\tilde{\mathrm{q}}$" could be β, γ and τ. The steering vector of the BS's receive UPA, namely $\mathbf{b}(\phi,\theta)$, is similarly defined as $\mathbf{a}(\phi,\theta)$ with N_{r_b} receive antennas. Symbols $\mathbf{b}_{n,0}$, $\mathbf{b}_{n,\tilde{k},\tilde{l}}$ and $\mathbf{b}_{n,i}$ denote the receive steering vector for the LoS path, NLoS paths, and clutters, where the clutter is assumed to be independently distributed over a set $\mathbf{\Omega}$ with interference-to-noise ratio $E[|\tilde{\beta}|^2]/\sigma_s^2$ [8].

The reflected echoes received at the BS can be formulated as $\mathbf{c}_n(t) = \tilde{\kappa}\sqrt{p_n}\tilde{\mathbf{w}}_n^H\tilde{\mathbf{H}}_n\mathbf{s}_n(t) + \mathbf{z}_s(t)$, where $\tilde{\kappa} = \sqrt{N_t N_{r_b}}$, $\tilde{\mathbf{w}}_n^H$ is the receive beamformer, and $\mathbf{z}_s(t)$ is the zero-mean Gaussian noise with variance σ_s^2. Note that the clutter components are regarded as interference, we thus have the signal-to-clutter-plus-noise ratio (SCNR) $\tilde{\Gamma}_r = p_n|\tilde{\kappa}\tilde{\mathbf{w}}_n^H(\tilde{\mathbf{H}}_n^{\mathrm{L}}+\tilde{\mathbf{H}}_n^{\mathrm{N}})\mathbf{f}_n|^2/(p_n|\tilde{\kappa}\tilde{\mathbf{w}}_n^H\tilde{\mathbf{H}}_n^{\mathrm{C}}\mathbf{f}_n|^2+\sigma_s^2)$.

The distance and velocity can be estimated by implementing 2D-DFT with respect to the received signal at each antenna [9]. Specifically, by performing IFFT and FFT on the fast and slow-time domains, the estimations about delay $\hat{\tau}_n$ and Doppler frequency $\hat{\gamma}_n$ can be obtained by detecting peaks, yielding estimations for location and velocity

$$\begin{cases} \hat{\tau}_n = 2||\mathbf{p}_n - \mathbf{p}_b||/c + z_\tau \\ \hat{\gamma}_n = 2\mathbf{v}_n^T(\mathbf{p}_n - \mathbf{p}_b)f_c/(c||\mathbf{p}_n - \mathbf{p}_b||) + z_\gamma \end{cases}, \tag{2}$$

where $\mathbf{v}_n = [\mathrm{v}_n(1), \mathrm{v}_n(2), \mathrm{v}_n(3)]^T$ is the velocity of the target UAV, and z_τ and z_γ denote the measurement Gaussian noise with zero mean and variance of σ_1 and σ_2, respectively.

The DoA can be estimated by applying the MUSIC algorithm [9]. By processing the range profile at the l-th symbol, we have $\mathbf{R}_l = [\mathbf{r}_1, \ldots, \mathbf{r}_{N_{r_b}}]$. The covariance matrix is given by $\mathbf{Y} = \frac{1}{L}\sum_{l=1}^{L}\mathbf{R}_l^{\mathrm{H}}\mathbf{R}_l$, and it can be further presented as $\mathbf{Y} = \mathbf{U_s}\mathbf{\Lambda_s}\mathbf{U_s}^H + \mathbf{U_n}\mathbf{\Lambda_n}\mathbf{U_n}^H$ via eigenvalue decomposition, where $\mathbf{\Lambda_s}$ and $\mathbf{\Lambda_n}$ are diagonal matrices that contain $\tilde{K}\tilde{L}$ and $N_{r_b} - \tilde{K}\tilde{L}$ eigenvalues. The MUSIC spectrum is calculated by $P_{\mathrm{MUSIC}}(\phi,\theta) = 1/(\mathbf{b}^H(\phi,\theta)\mathbf{U_n}\mathbf{U_n}^H\mathbf{b}(\phi,\theta))$. The angle can be estimated by traversing all the possible directions of the receive steering vector, and the estimation errors of $\hat{\theta}$ and $\hat{\phi}$ are Gaussian noise with zero mean and variance of σ_3 and σ_4.

III. Predictive and Fine Beamforming via EKF

Our solution is initialized by accessing UAV to BS, which can be easily realized by conventional beam training. Then the state prediction and tracking will continue for a long period of time. The signal transmitted by the BS is received by the UAV's UPA and also reflected by the fuselage. The reflected echos are exploited to measure the motion parameters at the last slot and perform one-step prediction by using the kinematic equations of the UAV. In addition, a fine tracking procedure will be performed based on the prediction result of EKF. Accordingly, the BS formulates transmit beamformer $\mathbf{f}_n$ based on the final tracked angles $\theta_{n|n-1}$ and $\phi_{n|n-1}$.

A. EKF-Based Predictive Beamforming

In this subsection, a Kalman filtering scheme is proposed for beam prediction and tracking. Due to the non-linearity in the measurement function, the linear Kalman filtering can not be utilized directly. We thus develop an EKF method that performs linearization for nonlinear measurement.

The state variables and measured vectors are denoted as $\boldsymbol{x}_n = [\mathbf{p}_n, \mathbf{v}_n, \mathbf{ac}_n]^T$ and $\boldsymbol{y}_n = [\tau_n, \gamma_n, \theta_n, \phi_n]^T$. The motions of UAV are regarded to keep constant within ΔT, the models of state evolution and measurement can be given by $\boldsymbol{x}_n = \mathbf{G}\boldsymbol{x}_{n-1} + \boldsymbol{z}_n$ and $\boldsymbol{y}_n = \mathbf{F}(\boldsymbol{x}_n) + \boldsymbol{z}'_n$, where $\mathbf{G} = [\mathbf{I}_{3\times3}, \Delta T\cdot\mathbf{I}_{3\times3}, \frac{\Delta T}{2}\cdot\mathbf{I}_{3\times3}; \mathbf{0}_{3\times3}, \mathbf{I}_{3\times3}, \Delta T\cdot\mathbf{I}_{3\times3}; \mathbf{0}_{3\times3}, \mathbf{0}_{3\times3}, \mathbf{I}_{3\times3}]$, and $\mathbf{F}(\cdot)$ is offered in Section II-B. Symbols $\boldsymbol{z}$ and $\boldsymbol{z}'$ are noises with covariance matrices as $\mathbf{Q}_s = \mathrm{diag}(\sigma^2_{\mathrm{p}(1)}, \sigma^2_{\mathrm{p}(2)}, \sigma^2_{\mathrm{p}(3)}, \sigma^2_{\mathrm{v}(1)}, \sigma^2_{\mathrm{v}(2)}, \sigma^2_{\mathrm{v}(3)}, \sigma^2_{\mathrm{ac}(1)}, \sigma^2_{\mathrm{ac}(2)}, \sigma^2_{\mathrm{ac}(3)})$ and $\mathbf{Q}_m = \mathrm{diag}(\sigma_1^2, \sigma_2^2, \sigma_3^2, \sigma_4^2)$.

According to [10], [11], the variances of the measurement noises are directly proportional to the Cramer-Rao bounds, which are inversely proportional to the SCNR, we thus model them as $\sigma_i^2 = a_i^2/\tilde{\Gamma}_r$, $i = 1 \sim 4$, with a_i being constants related to the system configuration, signal designs as well as the specific signal processing algorithms.[3]

In order to linearize the measurement models, the Jacobian matrix of $\mathbf{F}$ can be calculated by $[\frac{\partial\mathbf{F}}{\partial\boldsymbol{x}}, \mathbf{0}_{3\times3}]$, where

$$\frac{\partial\mathbf{F}}{\partial\boldsymbol{x}} = \begin{bmatrix} m(1) & m(2) & m(3) & 0 & 0 & 0 \\ \varrho(1) & \varrho(2) & \varrho(3) & \overline{m}(1) & \overline{m}(2) & \overline{m}(3) \\ \xi(1) & \xi(2) & \frac{\eta^2\xi(3)}{\mathrm{p}^2(3)} & 0 & 0 & 0 \\ \frac{\mathrm{p}(2)}{\eta^2} & \frac{\mathrm{p}(1)}{\eta^2} & 0 & 0 & 0 & 0 \end{bmatrix}, \tag{3}$$

$\eta = \sqrt{\mathrm{p}^2(1)+\mathrm{p}^2(2)}$, $m(i) = 2\mathrm{p}(i)/(c\sqrt{\mathbf{p}^T\mathbf{p}})$, $\varrho(i) = 2f_c[\mathrm{v}(i)\mathbf{p}^T\mathbf{p} - \mathrm{p}(i)\mathbf{p}^T\mathbf{v}]/(c(\mathbf{p}^T\mathbf{p})^{3/2})$, $\overline{m}(i) = f_c m(i)$, $\xi(i) = \mathrm{p}(i)\mathrm{p}(3)/(\mathbf{p}^T\mathbf{p}\sqrt{\mathbf{p}^T\mathbf{p} - \mathrm{p}^2(3)})$, $i = 1, 2, 3$.

The detailed steps of EKF are summarized as follows. 1) State prediction: $\hat{\boldsymbol{x}}_{n|n-1} = \mathbf{G}\boldsymbol{x}_{n-1}$. 2) Linearization by Eq. (3); 3) Predicting the mean squared error (MSE) matrix: $\mathbf{M}_{n|n-1} = \mathbf{G}_{n-1}\mathbf{M}_{n-1}\mathbf{G}_{n-1}^H + \mathbf{Q}_s$. 4) Calculating the

[3]Although there are other factors that affect the sensing accuracy, e.g., the bandwidth, duration of the signal, and smoothing window, we choose not to discuss them in this letter, for the purpose of avoiding alleviating the focus of the multipath effect on the beamforming gain to analyzing estimation errors.

Algorithm 1 Predictive and Fine Beam Tracking

Require: $\mathbf{S}$; Initial estimations θ_0, ϕ_0, τ_0, γ_0
Ensure: Beamforming directions at each time slot
1: **for** n from 1 to N **do**
2: Transmit the ISAC signal via beamformer $\mathbf{a}(\theta_n, \phi_n)$
3: Estimate θ_n, ϕ_n, τ_n, γ_n and β_n from radar echoes
4: Perform the EKF procedure
5: Determine the candidate set $\mathbf{S}$
6: **for** s from 1 to $|\mathbf{S}|$ **do**
7: Perform beam training
8: **end for**
9: Find the angle pairs with the highest SNR
10: Determine the transmit beamformer $\mathbf{a}(\theta_{n+1}, \phi_{n+1})$
11: **end for**

Kalman gain: $\mathbf{K}_n = \mathbf{M}_{n|n-1}\mathbf{F}_n^H(\mathbf{Q}_m + \mathbf{F}_n\mathbf{M}_{n|n-1}\mathbf{F}_n^H)^{-1}$. 5) State tracking: $\hat{\boldsymbol{x}}_n = \hat{\boldsymbol{x}}_{n|n-1} + \mathbf{K}_n(\boldsymbol{y}_n - \mathbf{F}(\hat{\boldsymbol{x}}_{n|n-1}))$. 6) Updating the MSE matrix: $\mathbf{M}_n = (\mathbf{I} - \mathbf{K}_n\mathbf{F}_n)\mathbf{M}_{n|n-1}$. By performing prediction iteratively, the BS can simultaneously sense and communicate with a relatively high SNR at low alignment costs, and we call this the EKF-ISAC method.

B. Fine Beam Tracking

The alignment angles after EKF may still deviate from the optimal one due to the following effects in the multipath channel. i) The radar sensing suffers larger errors due to the presence of clutters and ii) the communication DoF, namely the gain brought by the NLoS paths, is not fully utilized. It is therefore recommended to perform fine tracking based on the prediction result of EKF-ISAC. Taking the BS as an example, the steps are as follows. 1) Locating the baseline angles in the 2D azimuth elevation sparse grid [12] based on angles predicted by EKF. 2) Determining the cardinality $|\mathbf{S}|$ of the candidate set $\mathbf{S}$ on demand. 3) Determining $|\mathbf{S}|$ angle pairs clockwise from near to far based on the baseline angle pairs. 4) Traversing $|\mathbf{S}|$ angles in the candidate set to perform beam training, and regarding the angle pair with the highest SNR as the final alignment direction. A similar procedure will be performed by UAV with a candidate set $\mathbf{S}'$. The pseudo-code[4] of the proposed solution, which combines the EKF-ISAC and the fine beam tracking, is presented in **Algorithm** 1.

IV. Numerical Results

In this section, we run 1000 simulations and analyze the average results to respond to the three questions raised in the penultimate paragraph of Section I. The UAV's initial state is $\boldsymbol{x}_0 = [18, 50, 30, 0.8, -20, 0, -1, -1, -1]^T$, and we have $\sigma_{\mathrm{p}(i)} = 0.2m$, $\sigma_{\mathrm{v}(i)} = 0.1m/s$, $\sigma_{\mathrm{ac}(i)} = 0.05m/s^2$, $\forall i$. The BS is located at $(0m, 0m, 10m)$. Reference [6, Table 7.5-3] is introduced to define the ray offset DoA, and the multipath ADoAs are denoted as follows. For $\boldsymbol{x}_n(2) \geq 0$, $10^\circ \leq \phi'_{n,k} \leq 20^\circ$; for $\boldsymbol{x}_n(2) < 0$, $-20^\circ \leq \phi'_{n,k} \leq -10^\circ$; $45^\circ \leq \theta'_{n,k} \leq 55^\circ$, $k = 1, \ldots, K$. Besides, the EDoAs, ADoDs and EDoDs of the NLoS paths are generated in the same way as that for ADoAs. The Ricean K-factor is set as $\mathrm{K_R} = 1$. For the sensing channel, we randomly select $\tilde{K} = K/2$ clusters and $\tilde{L} = L/2$ from K clusters and their L paths to simplify the settings of sensing scatterers and regard them as useful paths that bring required sensing information. We generate $|\mathbf{\Omega}|$ clutters around the UAV's actual location with a maximum deviation of 5°. The angles in $\mathbf{S}$ are evenly distributed between 0 and 45°. Other parameters are shown in Table I.

TABLE I
Parameters of Simulation

Parameter	Value	Parameter	Value	Parameter	Value	Parameter	Value
f_c	28 GHz	c_{ASA}	22°	σ_c^2	-174 dBm	ΔT	0.05 s
p	23 dBm	$\sigma_{SF_{n,0}}$	4 dB	a_l	0.01	$\sigma_{SF_{n,k,l}}$	8.2 dB

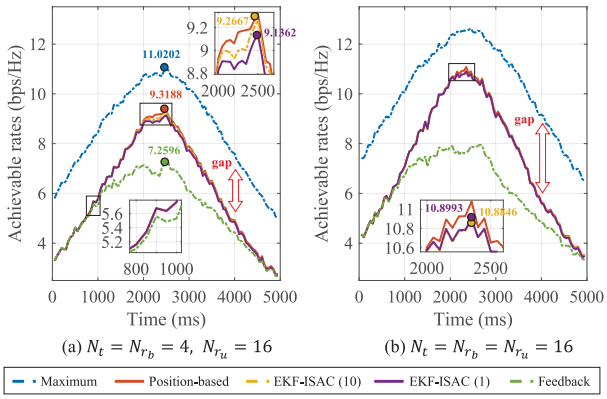

Fig. 2. Comparison of the achievable rate performances for various schemes with different numbers of antenna. $K = L = 10$. The numbers in brackets of legend denotes $|\mathbf{\Omega}|$, namely (1) and (10) means $|\mathbf{\Omega}| = 1$ and 10, respectively.

In Fig. 2, we first look at the achievable rates realized by the feedback-based method and the proposed EKF-ISAC method. Note that the "maximum" curve describes the largest rates with the optimal gain, which is found by global searching. The position-based curve describes the performance when the beam is aligned toward UAV's actual location. Note that UAV approaches BS between 2000ms and 3000 ms. During this period, the angles ϕ and θ change faster, and the beamforming gain of the feedback-based method drop owing to the following reasons: i) only one single pilot is being exploited for tracking, the small matched-filtering gain induces more significant measurement errors; ii) it quantifies the angles and feeds them back to the BS, which inevitably leads to the quantization errors and the estimation obtained from the previous slots may be outdated. Moreover, it becomes even worse when $N_t = N_{r_b} = N_{r_u} = 16$ due to the narrower beam and higher misalignment probability. In contrast, the EKF-ISAC solution utilizes the whole echo signal block for sensing, and the matched filter gain is more significant than the feedback-based one, resulting in a more minor measurement error. In addition, it makes consecutive angle estimations without quantization errors and thus accurate angular information can be preserved. As a result, it almost overlaps with the position-based curve, indicating a high estimation accuracy.

[4]The time consumption mainly lies in the fine beam tracking stage in rows 6∼8, and the time cost and alignment accuracy are remarkably affected by $|\mathbf{S}|$, which should be set as small (or large) as possible to perusing a better time efficiency (or alignment gain). Based on the baseline angles, $\lceil(|\mathbf{S}|-1)/2\rceil$ and $|\mathbf{S}| - \lceil(|\mathbf{S}|-1)/2\rceil - 1$ angle pairs are selected in descending and ascending order with an equal interval in the code book, respectively. If there are not enough angles on one side, use the angles on the other side to make up.

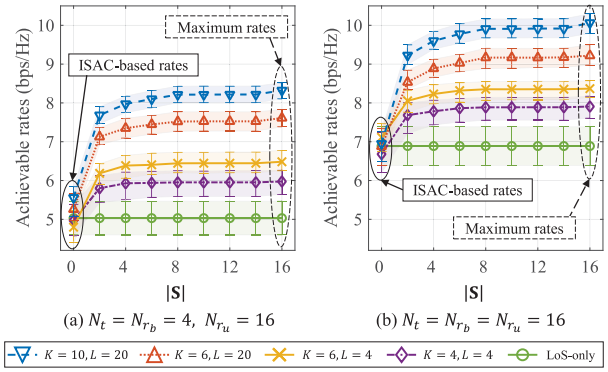

Fig. 3. Achievable rates versus the cardinality of $\mathbf{S}$ with different numbers of cluster, ray and antenna. The results are present with boxplot.

TABLE II
INFLUENCE OF THE NUMBER OF ANTENNA, CLUSTERS, AND PATHS ON THE PERFORMANCE GAP, $N_{r_u} = 16$

	$K = L = 4$	$K = 6, L = 4$	$K = 6, L = 20$	$K = 10, L = 20$
$N_t = N_{r_b} = 4$	17.66%	25.43%	31.42%	35.05%
$N_t = N_{r_b} = 16$	17.82%	26.28%	31.87%	35.21%

The ISAC-based schemes also significantly reduce the delay by removing the tedious feedback [1].

The cardinality $|\mathbf{\Omega}|$ has hardly any effect on the tracking performance of the EKF-ISAC. Although it affects $\tilde{\Gamma}_r$ and the resulting errors of measurement and tracking, the beamformer with slight deviation may enhance the gain of NLoS links and fully utilize the spatial DoF, which brings more channel gains. For the same reason, the aligned direction of EKF-ISAC has not yet enjoyed maximum gains before performing fine beam tracking. Specifically, the EKF-ISAC with $|\mathbf{\Omega}| = 1$ only averagely reaches 69.34% and 70.87% of the maximum rates when $N_t = N_{r_b} = 4$ and 16, respectively. This means that "seeing is not always believing", namely the angle parameters observed from radar echoes are not always the optimal alignment direction, even though they've been accurately tracked. Next, we will analyze the reason for this rate gap and the performance of the proposed fine-tracking method.

In Fig. 3, starting from the EKF-ISAC-based rates, the increasing $|\mathbf{S}|$ (i.e., the numbers of trained angles) makes it possible to reach higher rates in multipath environments, and the near-maximum rates could be reached when $|\mathbf{S}| = 16$. However, a large $|\mathbf{S}|$ means a longer training time. When considering both the BS and UAV simultaneously, $|\mathbf{S}|(|\mathbf{S}'| + 1)$ beam directions should be iterated, and each iteration requires a 5 ms time cost [7]. It can be remarkably reduced by cautiously selecting the beam set $\mathbf{S}$ and $\mathbf{B}'$ on demand.

Furthermore, there is no rate gap between the ISAC-based rates and the maximum rate in the LoS-only case since the real angles are the best-aligned directions. As shown in Table II, the rate gap increases with a larger K and L due to the increasing DoF, and there is hardly any gap difference with various N_t and N_{r_b} since they have few influences on the NLoS gain. Generally, the EKF-ISAC-based method has a nearly one-third gap from reaching the maximum rate when $K = 10$ and $L = 20$. The fluctuation of results caused by random channels did not have a significant impact on these conclusions.

Thanks to the channel gain brought by the spatial DoF, both the increasing K and L have a positive impact on the ISAC-based rates and the maximum rates. However, the ISAC-based rates in the multi-path channel are not significantly different from the LoS-only case, and even lower than the LoS-only rate when having a small K and L. The reason behind this is that although the CIR amplitude of the LoS path is generally higher than that of the NLoS path, the event that losing the LoS path still occasionally occurs according to Eq. (1). That means, the NLoS gain in cases with small K and L, is too small to compensate for the possibly missing LoS gain, which makes the achievable rate lower than the LoS-only case.

V. CONCLUSION

In this compact letter, we design a novel ISAC-assisted beam-tracking solution in multipath channels and shed light on its superiority to the feedback-based method. It also demonstrates that the angle parameters observed from radar echoes are not always the optimal alignment direction. The proposed fine beam tracking method could bridge this gap on demand at the cost of some beam training time. A more practical ISAC channel as well as the impact of its characteristics (such as scatterers position, spatial consistency for sensing, sensibility probability for selection, and RCS and angle spread within clusters) on the beam tracking performance are designated as our future work.

REFERENCES

[1] Y. Cui, Z. Feng, Q. Zhang, Z. Wei, C. Xu, and P. Zhang, "Toward trusted and swift UAV communication: ISAC-enabled dual identity mapping," *IEEE Wireless Commun.*, vol. 30, no. 1, pp. 58–66, Feb. 2023.
[2] Y. Cui et al., "Specific beamforming for multi-UAV networks: A dual identity-based ISAC approach," in *Proc. IEEE Int. Conf. Commun. (ICC)*, Roma, Italy, 2023, pp. 4979–4985.
[3] F. Liu, W. Yuan, C. Masouros, and J. Yuan, "Radar-assisted predictive beamforming for vehicular links: Communication served by sensing," *IEEE Trans. Wireless Commun.*, vol. 19, no. 11, pp. 7704–7719, Nov. 2020.
[4] Y. Li, F. Liu, Z. Du, W. Yuan, and C. Masouros, "ISAC-enabled V2I networks based on 5G NR: How much can the overhead be reduced?" 2023, *arXiv:2301.12787*.
[5] S. Lu, F. Liu, and L. Hanzo, "The degrees-of-freedom in monostatic ISAC channels: NLoS exploitation vs. reduction," *IEEE Trans. Veh. Technol.*, vol. 72, no. 2, pp. 2643–2648, Feb. 2023.
[6] *Study on Channel Model for Frequencies From 0.5 to 100 GHz, V14.3.0*, 3GPP Standard TR 38.901, 2017.
[7] A. Hu and J. He, "Position-aided beam learning for initial access in mmWave MIMO cellular networks," *IEEE Syst. J.*, vol. 16, no. 1, pp. 1103–1113, Mar. 2022.
[8] Z. Xu, C. Fan, and X. Huang, "MIMO radar waveform design for multipath exploitation," *IEEE Trans. Signal Process.*, vol. 69, pp. 5359–5371, Oct. 2021. [Online]. Available: https://ieeexplore.ieee.org/document/9562316
[9] M. Braun, C. Sturm, and F. K. Jondral, "On the single-target accuracy of OFDM radar algorithms," in *Proc. IEEE Int. Symp. Pers., Indoor Mobile Radio Commun.*, Toronto, ON, Canada, 2011, pp. 794–798.
[10] Q. He, R. S. Blum, and A. M. Haimovich, "Noncoherent MIMO radar for location and velocity estimation: More antennas means better performance," *IEEE Trans. Signal Process.*, vol. 58, no. 7, pp. 3661–3680, Jul. 2010.
[11] F. Foroozan, A. Asif, and Y. Jin, "Cramer-Rao bounds for time reversal MIMO radars with multipath," *IEEE Trans. Aerosp. Electron. Syst.*, vol. 52, no. 1, pp. 137–154, Feb. 2016.
[12] Q. Zhang, H. Sun, Z. Wei, and Z. Feng, "Sensing and communication integrated system for autonomous driving vehicles," in *Proc. IEEE Conf. Comput. Commun. Workshops (INFOCOM WKSHPS)*, Toronto, ON, Canada, 2020, pp. 1278–1279.